Rate-equation analysis of deterministic chaos in a laser with a saturable absorber

Takehisa Tohei, Maki Tachikawa,* and Tadao Shimizu
Department of Physics, Faculty of Science, The University of Tokyo, Bunkyo-ku, Tokyo-113, Japan
(Received 25 June 1991; revised manuscript received 10 December 1991)

The dynamics of a single-mode laser containing a saturable absorber in its cavity is investigated by means of the linear stability analysis of the rate equations of a recently proposed model. It is found that a single degree of freedom, which characterizes the saturation effect in the absorptive medium, well predicts whether the laser oscillation becomes chaotic or not.

PACS number(s): 42.50.Lc, 42.55.Lt

I. INTRODUCTION

The laser is a useful test bench for nonlinear dynamics. Instabilities and chaos have been observed in types of single- and multi-mode laser systems by adjusting the laser-control parameters [1]. Infrared gas lasers are especially promising systems to realize one-to-one correspondence between experiment and theory because of their simple energy-level structure and well-known parameters.

Recently deterministic chaos was observed in passive Q-switching (PQS) pulsation by use of a CO_2 or N_2O laser with a gaseous saturable absorber in its cavity [2–6]. The two-level model [7] and the four-level model [8,9] for the laser system were not successful in reproducing chaotic PQS, while the three-level–two-level model (the 3-2 model) proposed by Tachikawa *et al.* [10] has given successful interpretations of the observed behaviors of the unstable laser oscillation. In the 3-2 model, the vibrational relaxation from the lower laser level is considered to be an essential process to describe the laser dynamics. The numerical calculations well reproduce the observed chaotic PQS pulse shapes, its period-doubling route, and the periodic windows with detailed fidelity [2,4–6,11].

In the rate-equation analysis of the 3-2 model, characteristics of the PQS dynamics have been clarified by several theoretical approaches. DeTomasi *et al.* [5] investigated the structure of the strange attractor in the phase space, and classified the PQS instabilities depending on their behavior around the fixed points. By studying the bifurcation behavior, Lefranc, Hennequin, and Dangoisse [12] clarified that the chaotic PQS pulsation is a typical example of the Shil'nikov-type instability, as is observed in the Belousov-Zhabotinskii reactions [13].

In this paper, the physical process to cause chaos in the laser system is clarified by calculating the rates of divergence of the distance between two neighboring trajectories in the phase space. We introduce a parameter ρ which indicates the occurrence of chaos. Compared with the Lyapunov exponent [14], ρ has an explicit formula with laser parameters, which gives us a direct understanding of the physical process to cause the instability. It is revealed that the saturable absorber plays a key role to make the orbit unstable.

II. RATE-EQUATION MODEL

Figure 1 shows a schematic diagram of the 3-2 model for a CO_2 or N_2O laser with a saturable absorber (LSA) [10]. In this model, the laser medium is represented by three vibrational levels: the upper laser level (0,0,1), the lower laser level (1,0,0) or (0,2,0), and the ground level (0,0,0), where the numbers in parentheses represent vibrational quantum numbers of CO_2 normal modes. Individual rotational levels are not specified in the gain medium since the rotational relaxation is fast enough, and gives no appreciable effect to the laser dynamics. The vibrational relaxation processes are introduced among the three levels whose rates are denoted by R_{10}, R_{12}, and R_{20}. Continuous excitation is supplied mainly from the ground level to the upper laser level at the rate P. The absorber medium is represented simply by two rotation-vibration levels in resonance with the laser radiation. It is assumed that the populations in those levels approach the thermal equilibrium values at an equal relaxation rate r.

The laser system is described by four nonlinearly coupled rate equations for the photon density I, the population densities in the upper and lower laser levels M_1 and M_2, and the population density difference between the absorber levels N. The equations are written as follows for the properly normalized variables [10]:

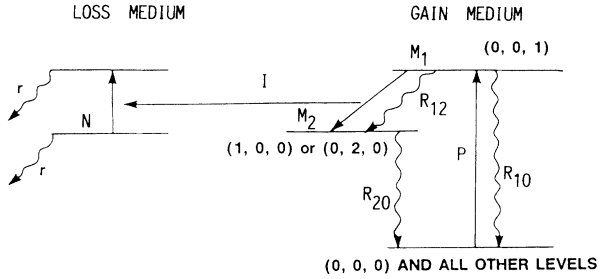

FIG. 1. Schematic representation of the three-level–two-level model for a laser with a saturable absorber. The laser medium is represented by three vibrational levels, and the absorber medium by two rotation-vibration levels.

$$\frac{dI}{dt}=(M_1-M_2-BN-k)I\ , \tag{1}$$

$$\frac{dM_1}{dt}=-(M_1-M_2)I+P(M-M_1-M_2) -(R_{10}+R_{12})M_1\ , \tag{2}$$

$$\frac{dM_2}{dt}=(M_1-M_2)I+R_{12}M_1-R_{20}M_2\ , \tag{3}$$

$$\frac{dN}{dt}=-2bNI-r(N-1)\ , \tag{4}$$

where

$$B=B_aN^*l_a/L\ , \tag{5}$$

$$b=B_a/(B_gf_g)\ . \tag{6}$$

The cavity loss rate is denoted by k. The coefficients B_g and B_a are the cross sections multiplied by the light speed for the induced emission in the gain medium and the absorption in the saturable absorber, respectively. The thermal equilibrium value of the population density difference in the absorber is denoted by N^*. L and l_a are the cavity length and the length of the absorption cell, respectively. f_g is the fraction of CO_2 or N_2O molecules in the rotational level from which the laser transition occurs.

III. CHAOS IN PASSIVE Q-SWITCHING PULSATION

The rate equations are numerically integrated by means of the fourth-order Runge-Kutta method. Figure 2 shows a phase diagram for the pumping rate P and the saturation parameter $2b/r$. The saturation parameter is proportional to the absorption cross section divided by the relaxation rate. Detailed structure of the parameter regions for regular pulsation, period doublings, and chaos is clearly seen in the phase diagram. As the saturation parameter becomes larger, the area for chaos gradually contracts and the width of the periodic window increases.

A typical chaotic pulse train is shown in Fig. 3(a). Parameter values used in the calculation appear in Table I. It is seen that single-, double-, and triple-peaked pulses appear in a random order in the chaotic time series.

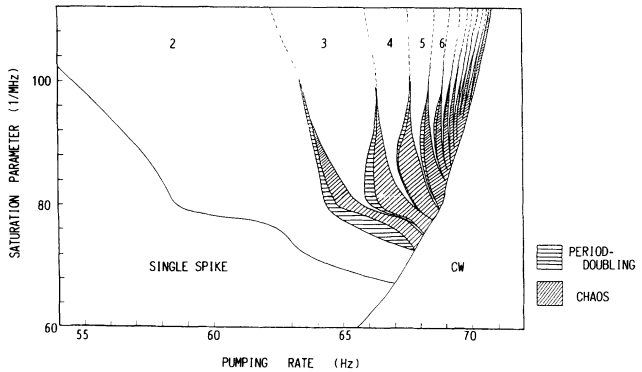

FIG. 2. Theoretically obtained phase diagram for the pumping rate and the saturation parameter where the regions for regular and chaotic PQS are depicted. The figures in the phase diagram indicate the number of peaks involved in a single PQS pulse.

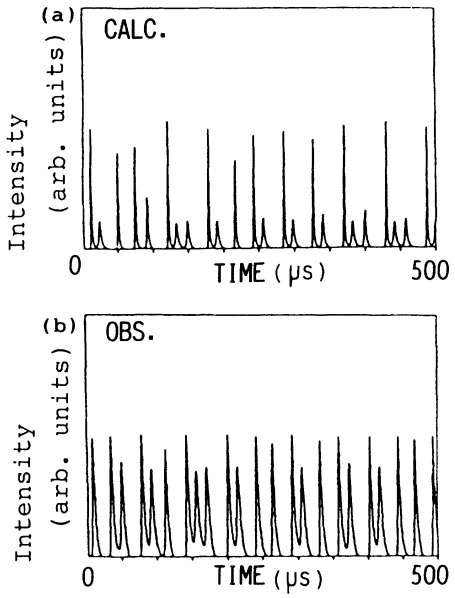

FIG. 3. Typical chaotic PQS pulsation numerically calculated on the three-level–two-level model (a), and chaotic PQS experimentally observed in a N_2O laser (b).

Basic features of the calculated pulse train such as the pulse shape and the pulsing frequency closely coincide with those of the chaotic PQS experimentally observed in a CO_2 and N_2O laser [4,6]. For comparison, a chaotic pulsation observed in a N_2O laser with an NH_3 absorber is shown in Fig. 3(b). It was previously confirmed that the rate-equation analysis also reproduced the characteristic dependence of the PQS behavior on the laser parameters such as the excitation current and the absorber pressure [4,6,10,11].

IV. LINEAR STABILITY ANALYSIS

Sensitive dependence of the trajectory on initial conditions results in the chaotic time evolution in a dynamical system [14]. The distance between two neighboring trajectories increases exponentially with time on the strange attractor. In this section, we derive a parameter which characterizes the rate of divergence of the neighboring trajectories in this LSA system under several approximations.

Here the population difference of the absorber $N(t)$

TABLE I. Parameter values used in the numerical calculation.

Parameter	Value
P	77.5 Hz
R_{10}	1.00 kHz
R_{12}	20.0 Hz
R_{20}	380.0 kHz
M	2000.0 MHz
k	2.50 MHz
B	2.50 MHz
b	500.0
r	0.50 MHz

can be eliminated adiabatically. Justification of the adiabatic elimination was discussed in the previous works [2,10]. Then, Eqs. (1)–(4) are rewritten as follows:

$$\frac{d\tilde{I}}{dt}=M_1-M_2-B/(1+e^{\tilde{I}}/I^*)-k\ , \tag{7}$$

$$\frac{dM_1}{dt}=-(M_1-M_2)e^{\tilde{I}}-(R_{10}+R_{12})M_1 +P(M-M_1-M_2)\ , \tag{8}$$

$$\frac{dM_2}{dt}=(M_1-M_2)e^{\tilde{I}}+R_{12}-R_{20}M_2\ , \tag{9}$$

where $\tilde{I}=\ln I$. $I^*=r/(2b)$, which denotes the saturation photon density for the absorber.

We introduce small deviation $\delta\mathbf{R}=(\delta\tilde{I}(t),\delta M_1(t),\delta M_2(t))$ from the original trajectory $\mathbf{R}=(\tilde{I}(t),M_1(t),M_2(t))$. In the linear approximation, the small deviation satisfies the following equations:

$$\frac{d}{dt}\begin{bmatrix}\delta\tilde{I}\\ \delta M_1\\ \delta M_2\end{bmatrix}=L\begin{bmatrix}\delta\tilde{I}\\ \delta M_1\\ \delta M_2\end{bmatrix}\ , \tag{10}$$

$$L=\begin{bmatrix}BI/(I+I/I^*)^2I^* & 1 & -1\\ -(M_1-M_2)I & -I-R_{10}-R_{12}-P & I-P\\ (M_1-M_2)I & I+R_{12} & -I-R_{20}\end{bmatrix}\ . \tag{11}$$

The divergence rate of $\delta\mathbf{R}$ in the direction of an eigenvector of the coefficient matrix L is defined by the real part of the corresponding eigenvalue.

The eigenvalues are analytically solved under the following approximations. Since R_{10}, R_{12}, and P are much smaller than R_{20} in the parameter values of interest (see Table I), L_{22}, L_{23}, and L_{32} are approximated to $-I$, I, and I, respectively. In the chaotic time series, $|L_{21}|$ and $|L_{31}|$ are much smaller than L_{11} unless $I\gg I^*$. L_{21}/L_{11} ranges between 0.04 and 0.1 when $I=I^*$, and takes smaller values for I lower than I^*. So, we set $L_{21}=L_{31}=0$. Then, the coefficient matrix is approximated to

$$L=\begin{bmatrix}BI/(1+I/I^*)^2I^* & 1 & -1\\ 0 & -I & I\\ 0 & I & -I-R_{20}\end{bmatrix}\ . \tag{12}$$

The eigenvalues of L are solved as

$$\lambda_0=\rho=BI/(1+I/I^*)^2I^*\ , \tag{13}$$

$$\lambda_\pm=-R_{20}/2-I\pm(I^2+R_{20}^2/4)^{1/2} \sim -I,-I-R_{20}\ . \tag{14}$$

Since $\lambda_\pm$ are always negative, the largest divergence rate is given by ρ. ρ is the derivative of the absorption rate in Eq. (7) with respect to $\tilde{I}$. Therefore ρ represents the strength of the feedback on the photon density caused by the saturable absorber. The mechanism to destabilize the orbit is now clear. Saturable loss gives a positive feedback to the laser system because the absorption coefficient of a saturable absorber is large for a weak electric field and small for a strong electric field. This saturation effect makes the orbit unstable.

Figure 4 shows temporal variations of the photon density [part (a)] and ρ [part (b)] calculated with the parameter values in Table I. The divergence rates numerically calculated from the coefficient matrix (11) without any approximations are represented by dashed curves in Fig. 4(b). The numerical solution reveals that one of the eigenvalues is always negative, and the other two are com-

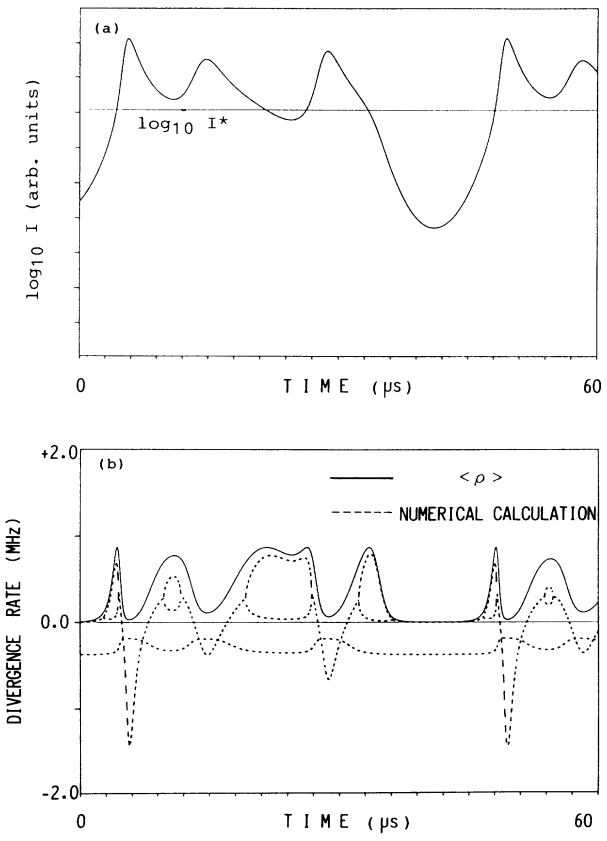

FIG. 4. Temporal variations of the photon density (a), and ρ (b) in the case of the chaotic PQS pulse train. Dashed curves represent numerically calculated divergence rates.

plex conjugate number or positive real numbers. Except when $I \gg I^*$, ρ agrees well with the largest one of the numerically calculated divergence rates, justifying the present approximation.

As a function of I, ρ takes the maximum value of $B/4$ at $I = I^*$. The numerical solution of the largest divergence rate also becomes maximum around $I = I^*$. Thus, a trajectory which stays long enough around I^* becomes chaotic. Typically, I^* is $\frac{1}{80}$ MHz in the parameter region for chaos. This corresponds to the radiation intensity of 20 W/cm^2, which is feasible in conventional CO_2 and N_2O lasers.

Figure 5(a) shows the mean value of ρ, $\langle \rho \rangle$, averaged over a sufficiently long period of time (1000 μs) as a function of the pumping rate P. For comparison, the Lyapunov exponents (LE's), generally accepted hallmarks of chaos, are obtained following the procedure of Wolf *et al.* [15]. One of the three LE's which characterizes the rate of divergence in the direction tangent to the trajectory is always zero in the present system. Chaos is realized in the parameter range where the larger one of the two other LE's is positive. The larger LE is also plotted in Fig. 5(b). There is a strong correlation between $\langle \rho \rangle$ and the Lyapunov exponent. The parameter ranges for chaos, where the Lyapunov exponent takes a positive value, well correspond to those with $\langle \rho \rangle$ larger than 0.35 MHz.

Figure 6(a) shows distribution of $\langle \rho \rangle$ over the parameter region of Fig. 2. Contour lines appear every 0.02 MHz. The thick contours correspond to $\langle \rho \rangle = 0.35$ MHz. A top view of Fig. 6(a) is shown in Fig. 6(b). The contour line $\langle \rho \rangle = 0.35$ MHz divides the parameter space into the regular PQS region (including the cw-mode region) and the chaos region (including the period doublings near chaos). Thus, instead of the Lyapunov exponents, we can use the parameter $\langle \rho \rangle$ to predict chaos in this LSA system.

It is interesting to note that an abrupt change in $\langle \rho \rangle$ well corresponds to the change in the regular PQS pulse shape. For example, $\langle \rho \rangle$ jumps by 0.07 MHz on the boundary between the single- and double-peaked pulses. This appears as a cliff in the top view. $\langle \rho \rangle$ also shows a drastic change when the PQS-mode oscillation turns into the cw-mode oscillation.

When the saturation parameter $2b/r$ is less than 70 MHz^{-1}, a discrepancy appears between the PQS behavior and the value of $\langle \rho \rangle$. In such a parameter region, a regular pulsation in the form of single spikes occurs even when $\langle \rho \rangle$ is larger than 0.35 MHz. At low saturation parameters, the largest divergence rate is not well approximated to ρ.

V. SUMMARY

Instability of a single-mode CO_2 or N_2O laser with a saturable absorber has been studied on the basis of the

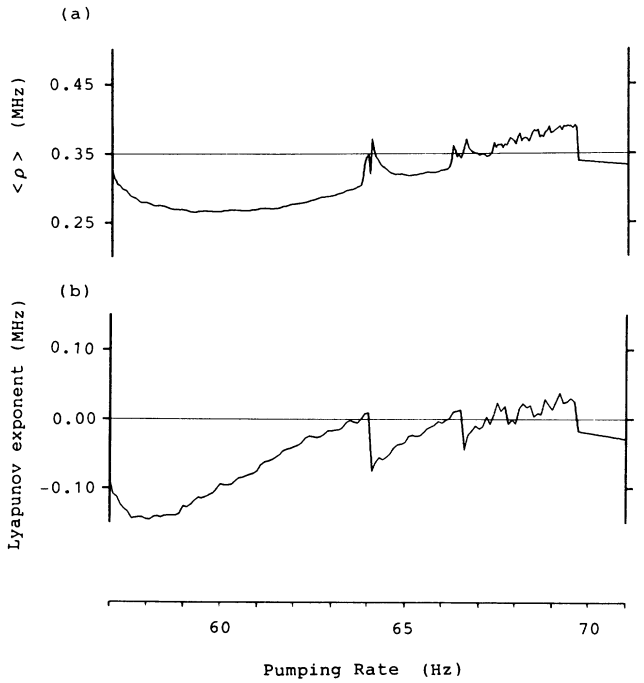

FIG. 5. Dependence of $\langle \rho \rangle$ (a) and the Lyapunov exponent (b) on the pumping rate. Chaos appears where the Lyapunov exponent is positive. In such parameter ranges, $\langle \rho \rangle$ takes relatively large values over 0.35 MHz.

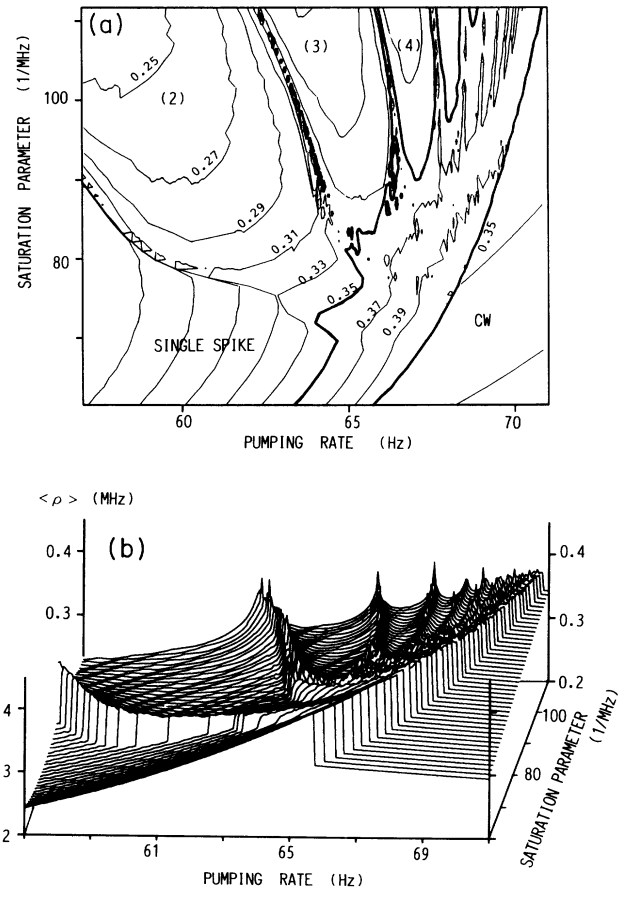

FIG. 6. (a) Distribution of $\langle \rho \rangle$ over the parameter region of Fig. 2. Contour lines are traced every 0.02 MHz. The figures in the parentheses indicate the number of peaks in a single PQS pulse. (b) Top view of (a). The cw-mode region and the single-spike region are separated from the other region by the two cliffs.

rate-equation model. The linear stability analysis of the rate equations was carried out. It has been found that the trajectory is destabilized by the saturation effect of the absorber, leading to chaos. The laser behavior is well characterized by a single parameter describing the degree of saturation of the absorber.

Generally, chaos is produced from nonlinear coupling of several variables, and a physical process responsible for chaos is not clearly interpreted except some special cases [16]. It is remarkable that the occurrence of chaos in the present laser system can be predicted by calculating the single parameter whose physical meaning is quite straightforward.

Compared with other systems such as the Lorenz model [17] and Rössler band [18], the PQS instability is easily accessible in a real experiment by use of conventional CO_2 and N_2O lasers. The PQS instability is a useful model to investigate fundamental aspects of the low-dimensional nonlinear system.

---

*FAX number: 81-3-5684-5291.

[1] *Instabilities and Chaos in Quantum Optics,* edited by F. T. Arecchi and R. G. Harrison (Springer-Verlag, Berlin, 1987).

[2] P. Gloreiux, J. Phys. (Paris) Colloq. **48**, C7-433 (1987). D. Dangoisse, A. Bekkali, F. Papoff, and P. Glorieux, Europhys. Lett. **6**, 335 (1988); A. Bekkali, F. Papoff, D. Dangoisse, and P. Glorieux, J. Phys. (Paris) Colloq. **49**, C2-349 (1988).

[3] D. Hennequin, F. DeTomasi, B. Zambon, and E. Arimondo, Phys. Rev. A **37**, 2243 (1988).

[4] M. Tachikawa, F.-L. Hong, K. Tanii, and T. Shimizu, Phys. Rev. Lett. **60**, 2266 (1988).

[5] F. DeTomasi, D. Hennequin, B. Zambon, and E. Arimondo, J. Opt. Soc. Am. B **6**, 45 (1989).

[6] F.-L. Hong, M. Tachikawa, R. Oda, and T. Shimizu, J. Opt. Soc. Am. B. **6**, 1378 (1989).

[7] H. T. Powell and G. J. Wolga, IEEE J. Quantum Electron. **QE-7**, 213 (1971).

[8] I. Burak, P. L. Houston, D. G. Sutton, and J. I. Steinfeld, IEEE J. Quantum Electron. **QE-7**, 73 (1971).

[9] E. Arimondo, F. Casagrande, L. A. Lugiato, and P. Glorieux, Appl. Phys. B **30**, 57 (1983).

[10] M. Tachnikawa, K. Tanii, M. Kajita, and T. Shimizu, Appl. Phys. B **39**, 83 (1986); M. Tachikawa, K. Tanii, and T. Shimizu, J. Opt. Soc. Am. B **4**, 387 (1987).

[11] M. Tachikawa, K. Tanii, and T. Shimizu, J. Opt. Soc. Am. B **5**, 1077 (1988).

[12] M. Lefranc, D. Hennequin, and D. Dangoisse, J. Opt. Soc. Am. B **8**, 239 (1991).

[13] F. Argoul, A. Arneodo, and P. Richetti, J. Chim. Phys. **84**, 1367 (1987).

[14] P. Berge, Y. Pomeau, and Ch. Vidal, *Order within Chaos* (Herman, Paris, 1984).

[15] A. Wolf, J. B. Swift, H. L. Swinney, and J. A. Vastano, Physics **16D**, 285 (1985).

[16] R. G. Brewer, J. Hoffnagle, R. G. DeVoe, L. Reyna, and W. Henshaw, Nature **344**, 305 (1990).

[17] E. N. Lorenz, J. Atmos. Sci. **20**, 130 (1963).

[18] O. E. Rössler, Phys. Lett. **57A**, 397 (1976).